SUPPORTING MATERIALS

DNA and BSA Interaction and DNA Cleavage and *in vitro* Cytotoxicity of Copper(II) Complexes: [Cu(bba)(phen)]$(ClO_4)_2$ is Promising Chemotherapeutic Scaffold

J. Manivel[1], S. Sangeetha[1,2], M. Murali[*,1]

[1]Coordination and Bioinorganic Chemistry Research Laboratory, Department of Chemistry National College (Autonomous), Tiruchirappalli 620 001Tamil Nadu, India

[2]Department of chemistry, Tamilavel Umamaheswaranar Karanthai Arts College, Thanjavur 613 002 Tamil Nadu, India

e-mail: ma66mu@gmail.com

Table S1

Electronic absorption and EPR spectral and electrochemical properties of Cu(II) complexes

Complex	λ_{max} in nm (ε, M^{-1} cm^{-1})		EPR spectra				Redox properties	
	Ligand field	Ligand based	Solid		Frozen DMF		DMF solution	
$[Cu(bba)(bpy)]^{2+}$ **1**	643 (70)	279 (33510)	g_{iso}	2.061	$g_{\|}$	2.249	$E_{1/2}$ (V, CV)	-0.074
		273 (32080)			$A_{\|}$	186	$E_{1/2}$ (V, DPV)	-0.081
		315 sh			$g_{\perp}$	2.053	ΔE_p (mV)	198
					$g_{\|}/A_{\|}$	122	i_{pa}/i_{pc}	0.9
					G	4.9	D (10^6 cm^2 s^{-1})	7.4
$[Cu(bba)(phen)]^{2+}$ **2**	639 (125)	279 (57250)	g_{iso}	2.053	$g_{\|}$	2.254	$E_{1/2}$ (V, CV)	-0.074
		273 (54390)			$A_{\|}$	182	$E_{1/2}$ (V, DPV)	-0.077
		314 sh			$g_{\perp}$	2.054	ΔE_p (mV)	128
					$g_{\|}/A_{\|}$	124	i_{pa}/i_{pc}	1.0
					G	4.9	D (10^6 cm^2 s^{-1})	7.6
$[Cu(bba)(dpa)]^{2+}$ **3**	667 (120)	315 (14800)	g_{iso}	2.066	$g_{\|}$	2.242	$E_{1/2}$ (V, CV)	-0.072
		269 (40540)			$A_{\|}$	181	$E_{1/2}$ (V, DPV)	-0.083
					$g_{\perp}$	2.049	ΔE_p (mV)	206
					$g_{\|}/A_{\|}$	124	i_{pa}/i_{pc}	0.9
					G	5.1	D (10^6 cm^2 s^{-1})	7.8

Table S2

Ligand-based absorption spectral properties[a] and fluorescence spectral properties[b] of copper(II) complexes bound to CT DNA

Complex	λ_{max} (nm)	R	Change in Absorbance	$\Delta\varepsilon$ (%)	K_b ($\times 10^4$ M^{-1})	K_{app} ($\times 10^5$ M^{-1})
$[Cu(bba)(bpy)](ClO_4)_2$ **1**	270	25	Hypochromism	48	3.2 ± 0.1	1.5
$[Cu(bba)(phen)](ClO_4)_2$ **2**	272	25	Hypochromism	61	3.4 ± 0.1	2.0
$[Cu(bba)(dpa)](ClO_4)_2$ **3**	277	25	Hypochromism	56	3.1 ± 0.1	1.0

[a]Measurements were made at R = 25, where R = [DNA]/[complex], concentration of solutions of copper(II) complexes = 2.5-2.7 $\times 10^{-5}$ M (**1**-**3**).
[b]Apparent DNA binding constant from ethidium bromide displacement assay using increasing concentration (0-10 μM) of **1**-**3**.

Table S3

Electrochemical behaviour[a,b] of the copper(II) complexes on interaction with CT DNA (r = [base-pair]/[Cu(II) complex]

	r	E_{pc} (V)	E_{pa} (V)	$E_{½}$ (V)		i_{pc}/i_{pc}	ΔE_p (mV)	$\Delta E_{1/2}$ (V)	K_+/K_{2+}
				CV	DPV				
1	0	-0.144	-0.034	-0.089	-0.083	1.0	110	-106	0.02
	5	-0.271	-0.115	-0.193	-0.189	1.0	156		
2	0	-0.155	-0.027	-0.091	-0.084	1.2	128	-104	0.02
	5	-0.255	-0.126	-0.191	-0.188	1.1	129		
3	0	-0.140	-0.029	-0.085	-0.076	1.0	111	-127	0.01
	5	-0.261	-0.145	-0.198	-0.203	1.2	116		

[a]Measured vs. SCE; scan rate: 50 mV s^{-1}; supporting electrolyte: 2% DMF - 5 mM Tris-HCl/50 mM NaCl; complex concentration: 0.5×10^{-3} M.
[b]Differential pulse voltammetry (DPV), scan rate 2 mV s^{-1}, pulse height 50 mV.

Table S4

Quenching, association, binding and thermodynamic parameters of the interaction of **1**-**3** with BSA at different temperatures[a]

Parameters	300 K	R	310 K	R
[Cu(bba)(bpy)]$(ClO_4)_2$ 1				
K_{SV} (10^5 M^{-1}) ± SD	3.164 ± 0.002	0.9995	3.582 ± 0.003	0.9989
k_q (10^{13} M^{-1} s^{-1})	3.164		3.582	
K_a (10^5 M^{-1}) ± SD	2.065 ± 0.031	0.9980	2.311 ± 0.014	0.9996
K_b (10^5 M^{-1}) ± SD	0.830 ± 0.112	0.9954	0.420 ± 0.048	0.9990
n ± SD	0.877 ± 0.018		0.860 ± 0.008	
ΔH° (kJ mol^{-1})	79.210			
ΔS° (J mol^{-1} K^{-1})	1O3.373		100.910	
ΔG° (kJ mol^{-1})	-30.932		-30.203	
[Cu(bba)(phen)]$(ClO_4)_2$ 2				
K_{SV} (10^5 M^{-1}) ± SD	2.451 ± 0.005	0.9986	2.786 ± 0.003	0.9993
k_q (10^{13} M^{-1} s^{-1})	2.451		2.786	
K_a (10^5 M^{-1}) ± SD	1.739 ± 0.026	0.9980	2.138 ± 0.032	0.9980
K_b (10^5 M^{-1}) ± SD	0.730 ± 0.121	0.9943	0.606 ± 0.061	0.9986
n ± SD	0.859 ± 0.020		0.875 ± 0.010	
ΔH° (kJ mol^{-1})	77.833			
ΔS° (J mol^{-1} K^{-1})	101.741		101.070	
ΔG° (kJ mol^{-1})	-30.444		-31.254	
[Cu(bba)(dpa)]$(ClO_4)_2$ 3				
K_{SV} (10^5 M^{-1}) ± SD	2.008 ± 0.006	0.9984	2.154 ± 0.006	0.9982
k_q (10^{13} M^{-1} s^{-1})	2.008		2.154	
K_a (10^5 M^{-1}) ± SD	1.046 ± 0.017	0.9992	2.209 ± 0.022	0.9991
K_b (10^5 M^{-1}) ± SD	1.426 ± 0.064	0.9986	0.789 ± 0.062	0.9986
n ± SD	0.897 ± 0.010		0.878 ± 0.010	
ΔH° (kJ mol^{-1})	78.066			
ΔS° (J mol^{-1} K^{-1})	102.188		101.212	
ΔG° (kJ mol^{-1})	-30.578		-31.298	

[a]R is the linear correlated coefficient.

Table S5

Förster's energy transfer parameters of the interaction of Cu(II) complexes with BSA

	E	$J \times 10^{15}$ (M^{-1} cm^{-1})	R_0 (nm)	r (nm)
1	0.18	4.33	1.46	6.61
2	0.09	8.02	3.18	3.80
3	0.08	3.08	2.06	2.14

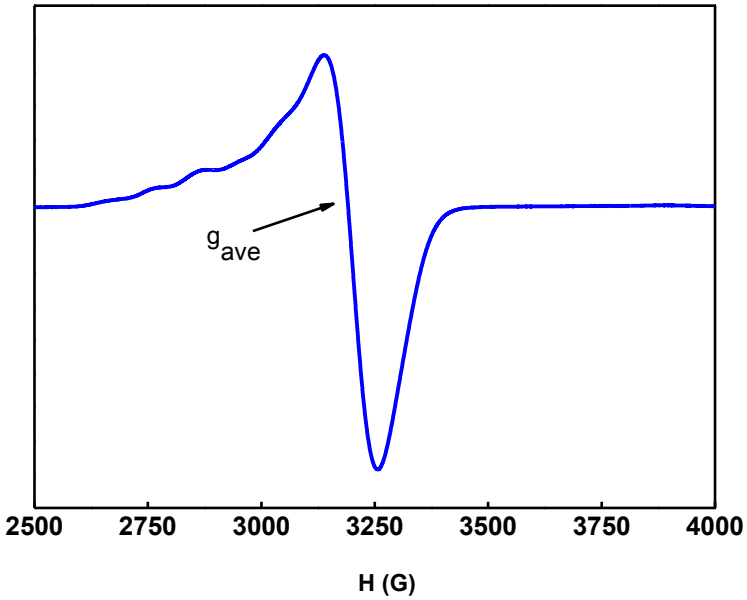

Fig. S1. Polycrytalline EPR spectrum of [Cu(bba)(bpy)]$(ClO_4)_2$ **1** at room temperature.

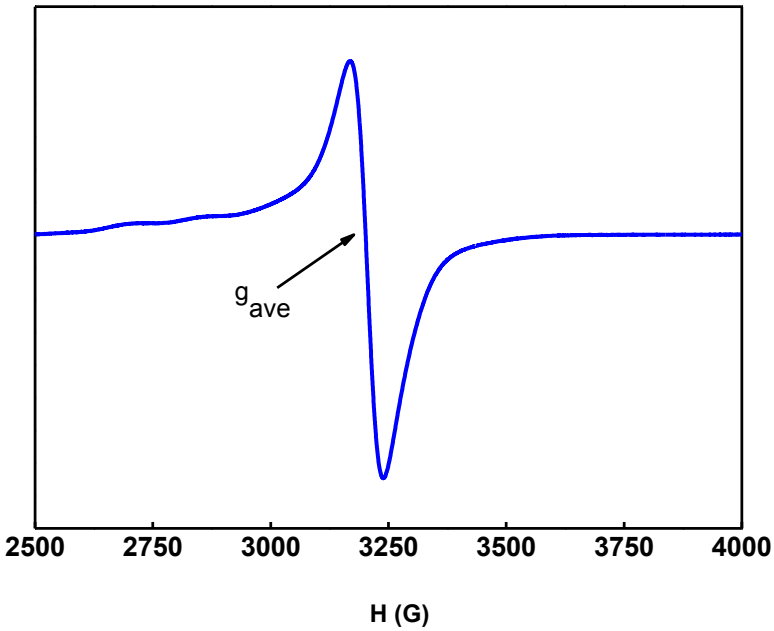

Fig. S2. Polycrytalline EPR spectrum of [Cu(bba)(phen)]$(ClO_4)_2$ **2** at room temperature.

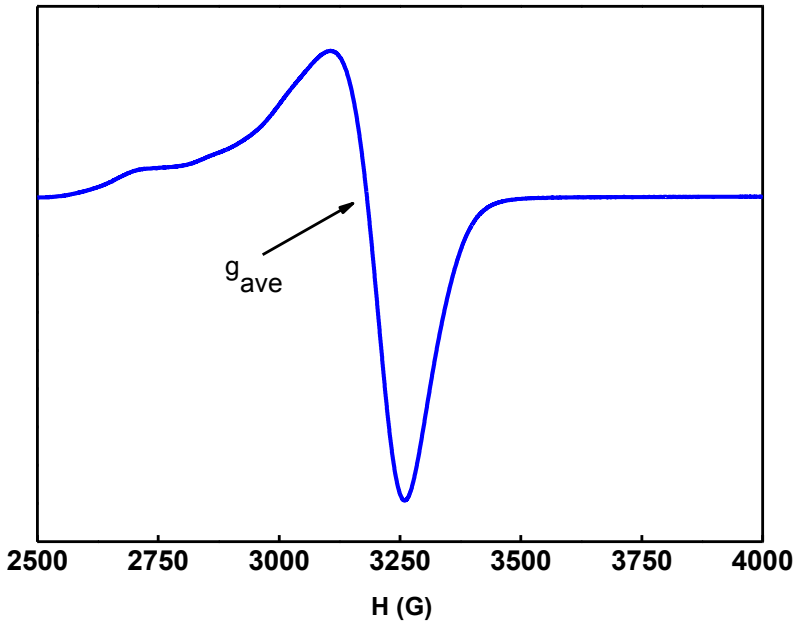

Fig. S3. Polycrytalline EPR spectrum of [Cu(bba)(dpa)]$(ClO_4)_2$ **3** at room temperature.

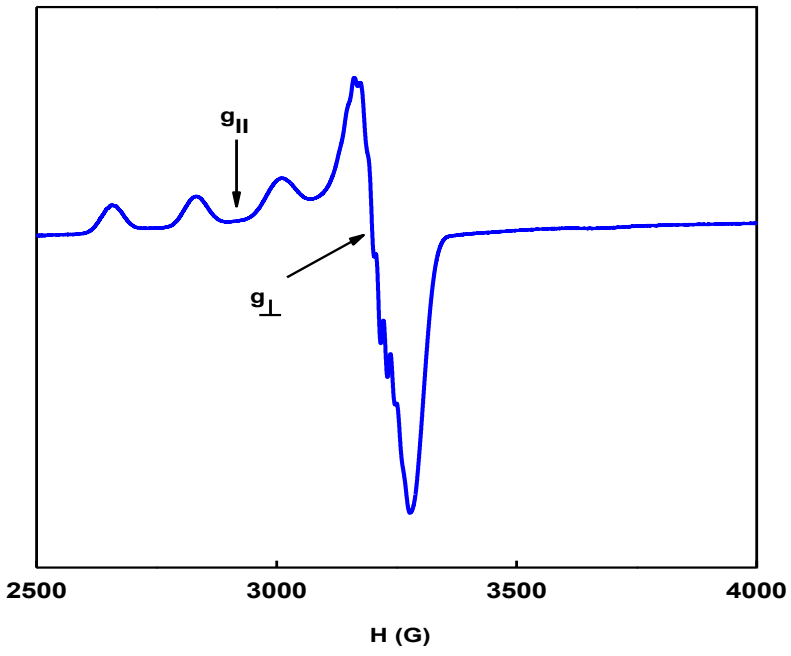

Fig. S4. EPR spectrum of [Cu(bba)(bpy)]$(ClO_4)_2$ **1** in DMF solution at 77 K (Microwave frequency: 9.185 GHz).

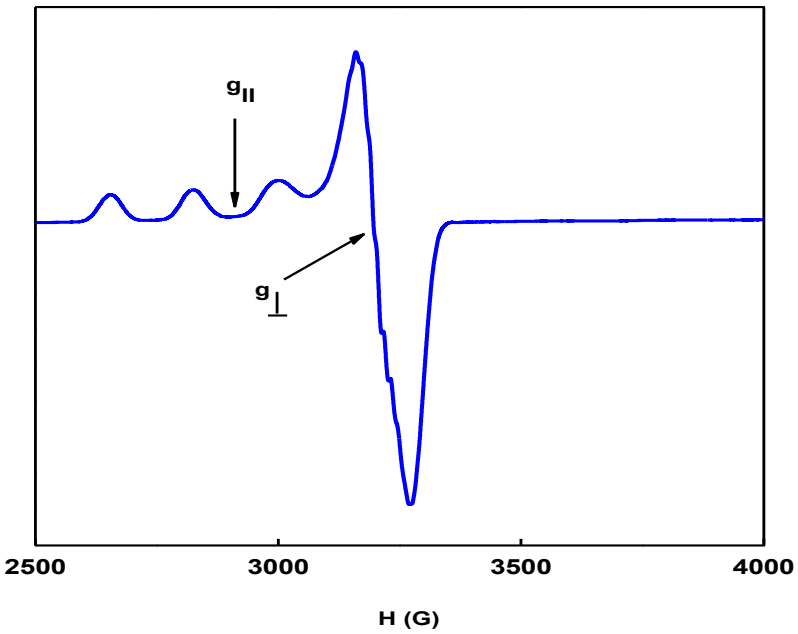

Fig. S5. EPR spectrum of [Cu(bba)(phen)]$(ClO_4)_2$ **2** in DMF solution at 77 K (Microwave frequency: 9.177 GHz).

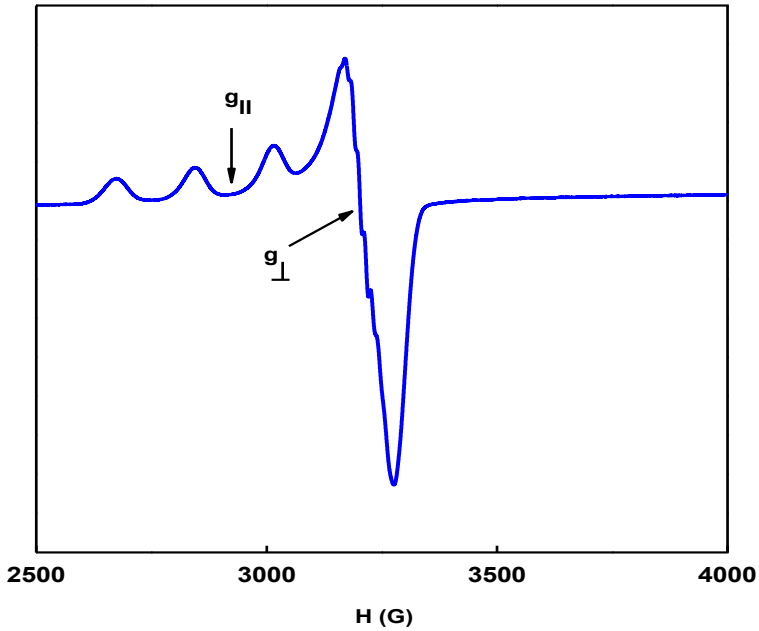

Fig. S6. EPR spectrum of [Cu(bba)(dpa)]$(ClO_4)_2$ **3** in DMF solution at 77 K (Microwave frequency: 9.187 GHz).

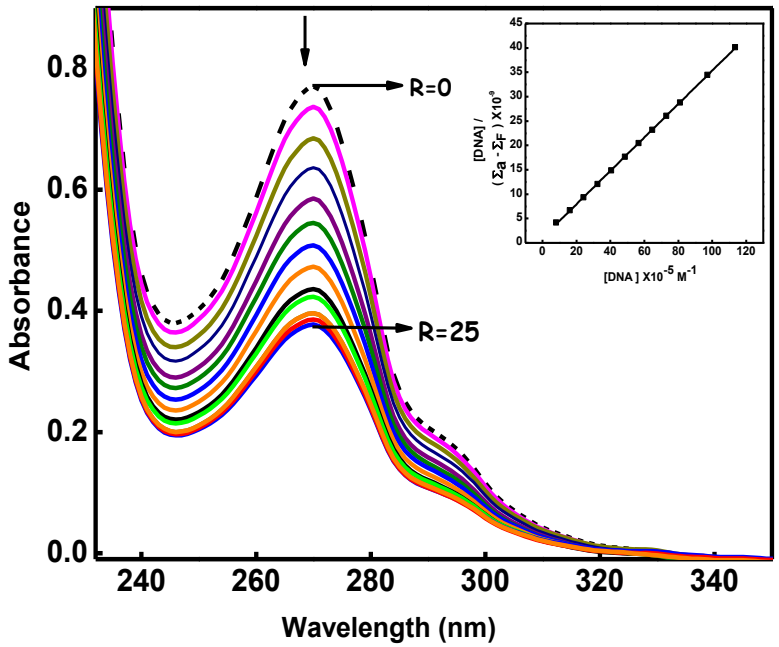

Fig. S7. Absorption spectra of **1** (2.5×10^{-5} M) in 2% DMF/5mM Tris-HCl/50 mM NaCl buffer at pH 7.1 in the absence (R = 0) and presence (R = 25) of increasing amounts of CT DNA. Inset: Plot of [DNA] vs [DNA]/(ε_a - ε_f) at R = 25 of **1**.

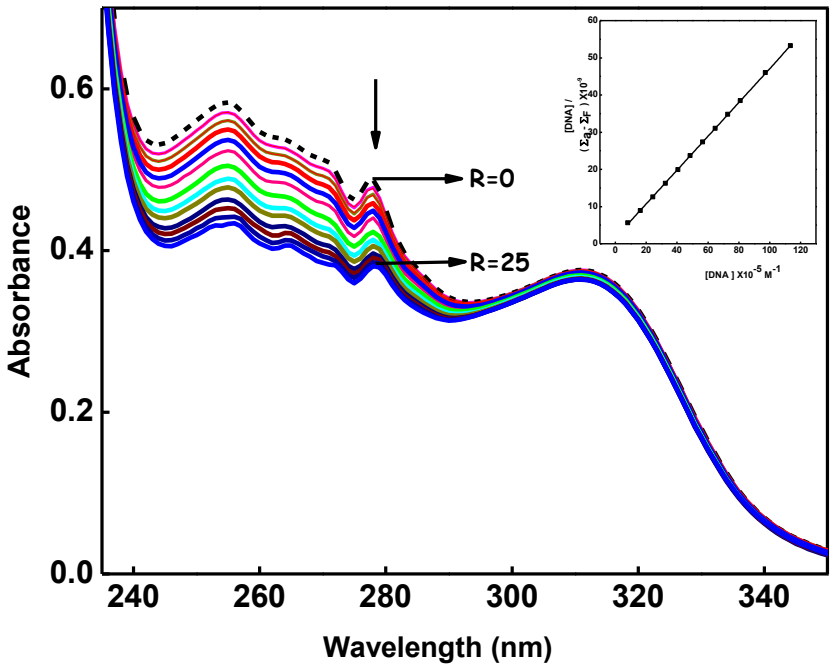

Fig. S8. Absorption spectra of **3** (2.7×10^{-5} M) in 2% DMF/5mM Tris-HCl/50 mM NaCl buffer at pH 7.1 in the absence (R = 0) and presence (R = 25) of increasing amounts of CT DNA. Inset: Plot of [DNA] vs [DNA]/(ε_a - ε_f) at R = 25 of **3**.

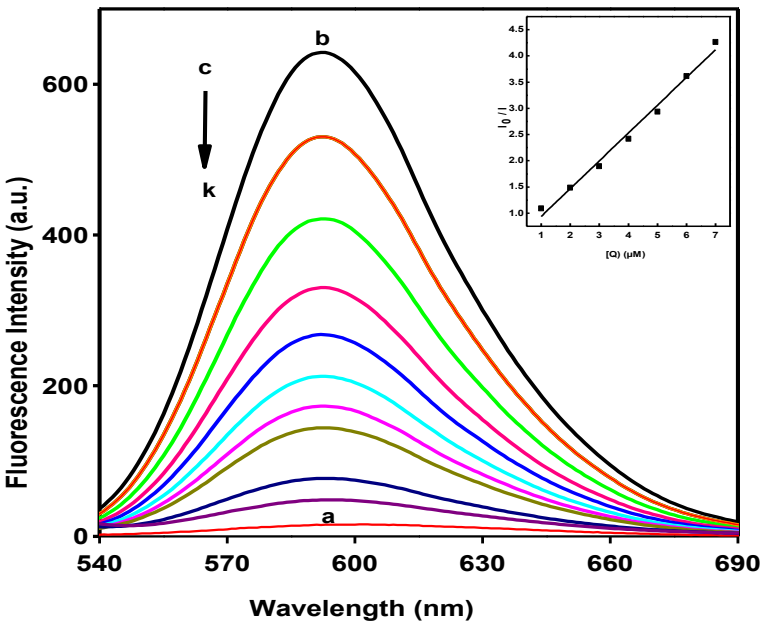

Fig. S9. Fluorescence quenching curves of ethidium bromide bound to DNA in 2% DMF/5mM Tris-HCl/50 mM NaCl buffer at pH 7.1: (a) EthBr (1.25 μM); (b) EthBr + DNA (125 μM); (c-k) EthBr + DNA + **1** (0-6 μM). Inset: Plot of [complex × 10^{-6}] vs I_O/I of **1**.

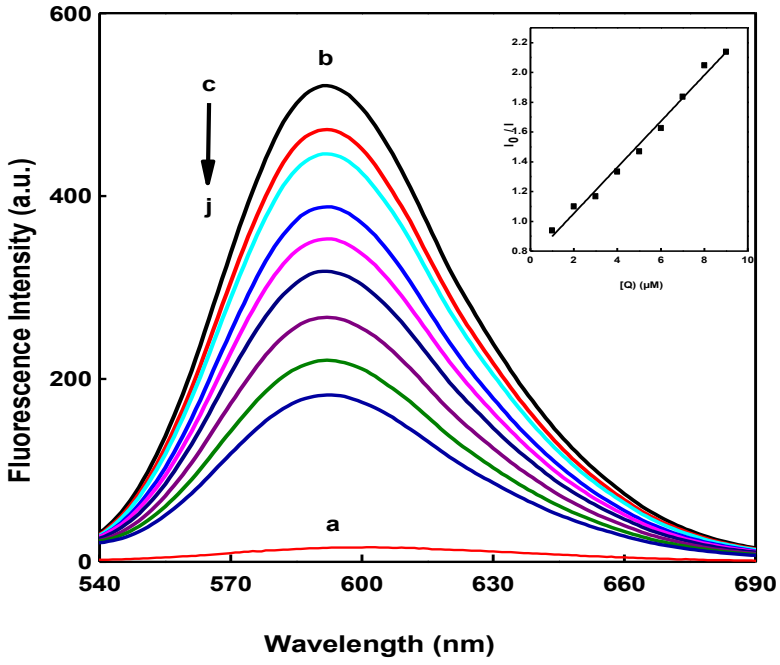

Fig. S10. Fluorescence quenching curves of ethidium bromide bound to DNA in 2% DMF/5mM Tris-HCl/50 mM NaCl buffer at pH 7.1: (a) EthBr (1.25 μM); (b) EthBr + DNA (125 μM); (c-j) EthBr + DNA + **3** (0-6 μM). Inset: Plot of [complex × 10^{-6}] vs I_O/I of **3**.

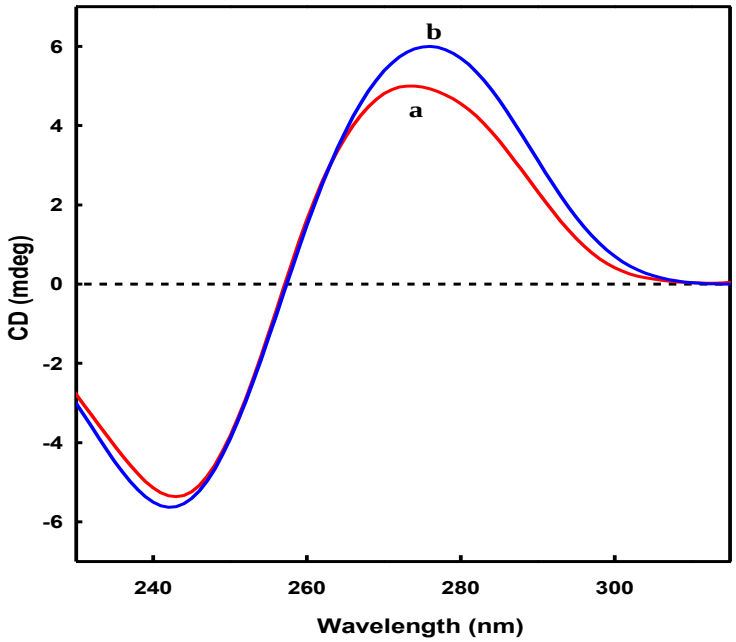

Fig. S11. Circular dichroism spectra of CT DNA in 2% DMF/5mM Tris-HCl/50 mM NaCl buffer at pH 7.1 and 25 °C in absence (a) and presence (b) of **1** at 1/R value of 3.

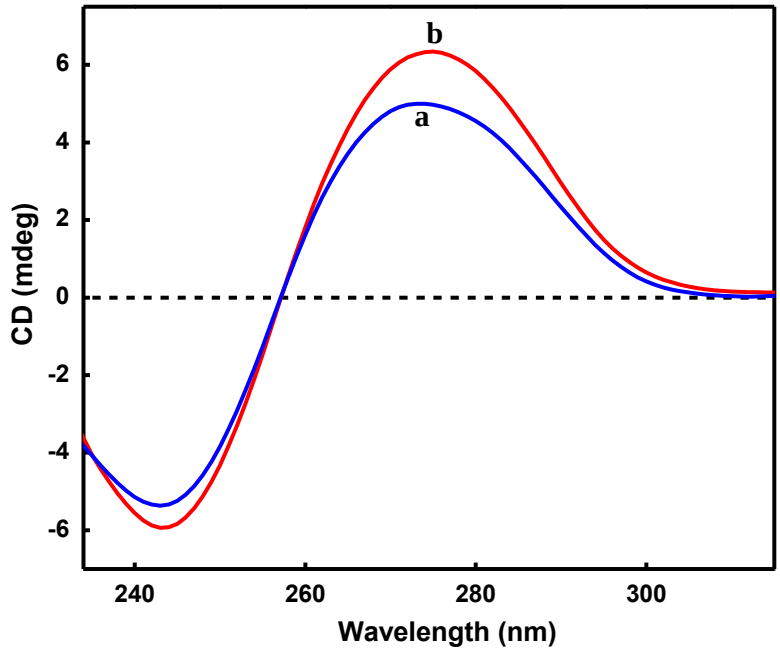

Fig. S12. Circular dichroism spectra of CT DNA in 2% DMF/5mM Tris-HCl/50 mM NaCl buffer at pH 7.1 and 25 °C in absence (a) and presence (b) of **3** at 1/R value of 3.

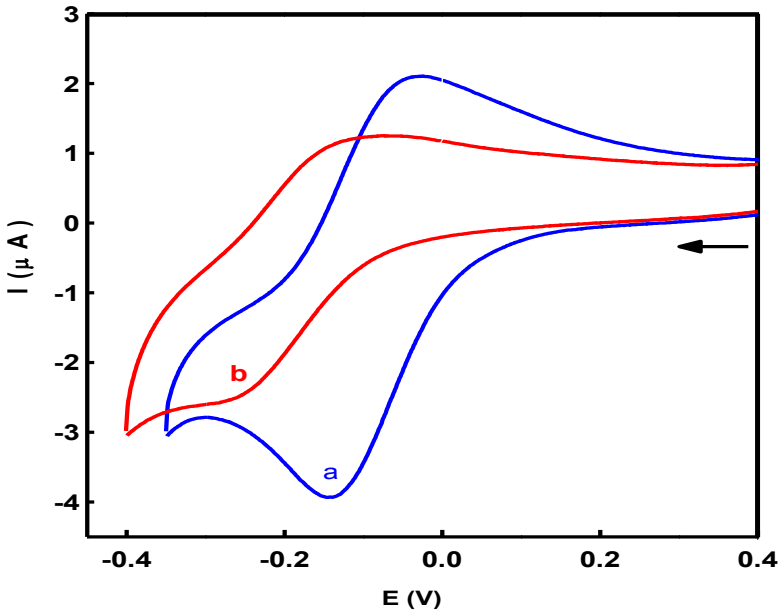

Fig. S13. Cyclic voltammograms of **1** (0.5 mM) in the absence (a) and presence (b) of CT DNA (R = 5) at 25.0 ± 0.2 °C at 50 mV s^{-1} scan rate in 2% DMF/5mM Tris-HCl/50 mM NaCl buffer at pH 7.1.

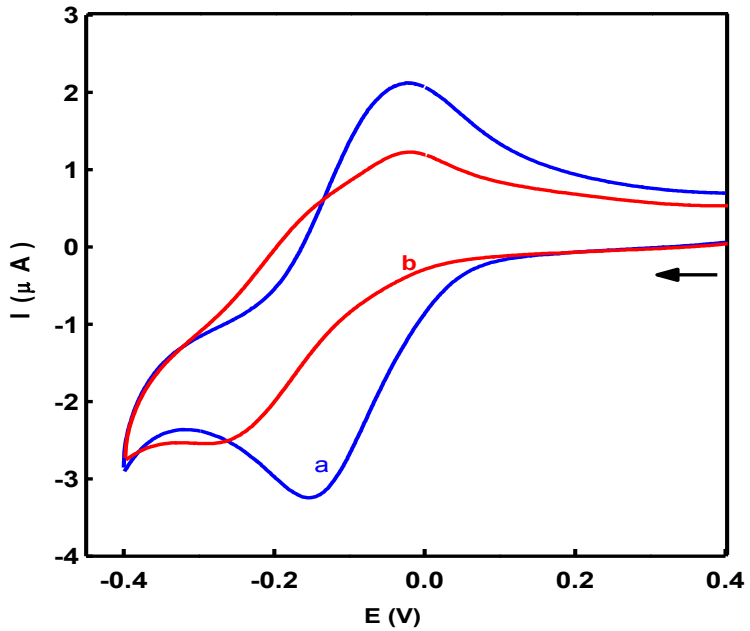

Fig. S14. Cyclic voltammograms of **2** (0.5 mM) in the absence (a) and presence (b) of CT DNA (R = 5) at 25.0 ± 0.2 °C at 50 mV s^{-1} scan rate in 2% DMF/5mM Tris-HCl/50 mM NaCl buffer at pH 7.1.

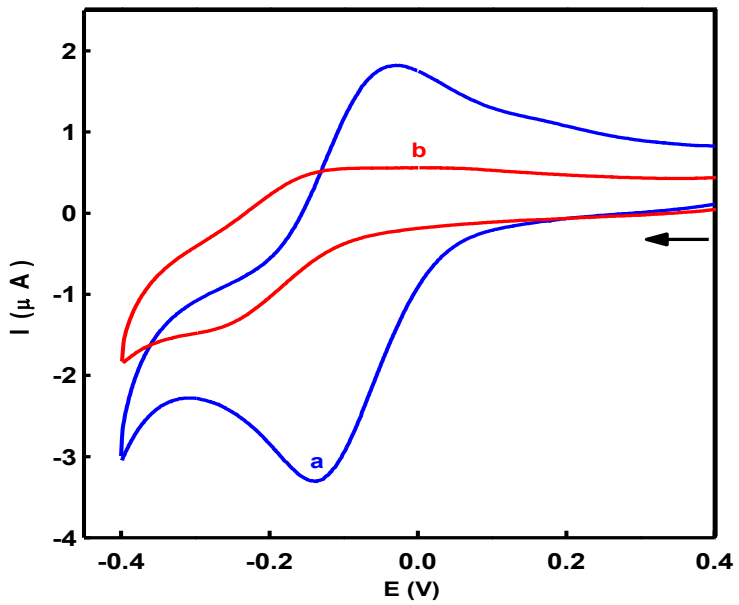

Fig. S15. Cyclic voltammograms of **3** (0.5 mM) in the absence (a) and presence (b) of CT DNA (R = 5) at 25.0 ± 0.2 °C at 50 mV s^{-1} scan rate in 2% DMF/5mM Tris-HCl/50 mM NaCl buffer at pH 7.1.

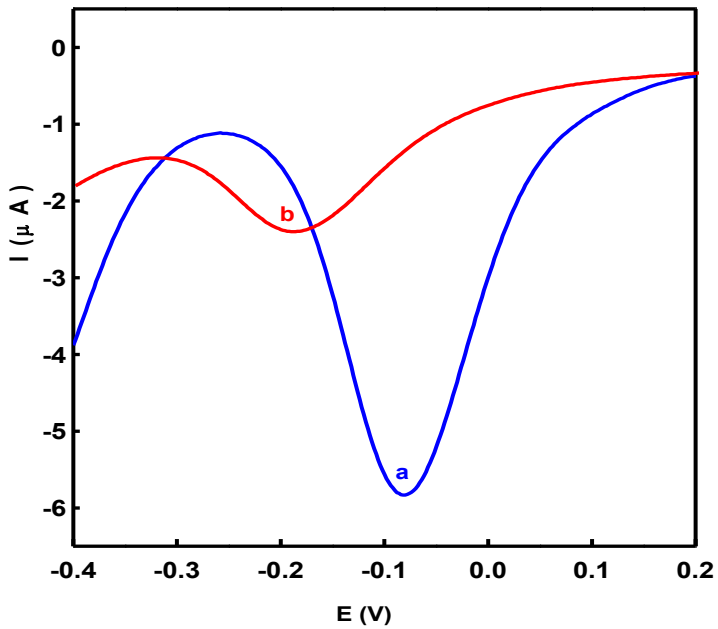

Fig. S16. Differential pulse voltammograms of **1** (0.5 mM) in the absence (a) and presence (b) of CT DNA (R = 5) at 25.0 ± 0.2 °C at 2 mV s^{-1} scan rate in 2% DMF/5mM Tris-HCl/50 mM NaCl buffer at pH 7.1.

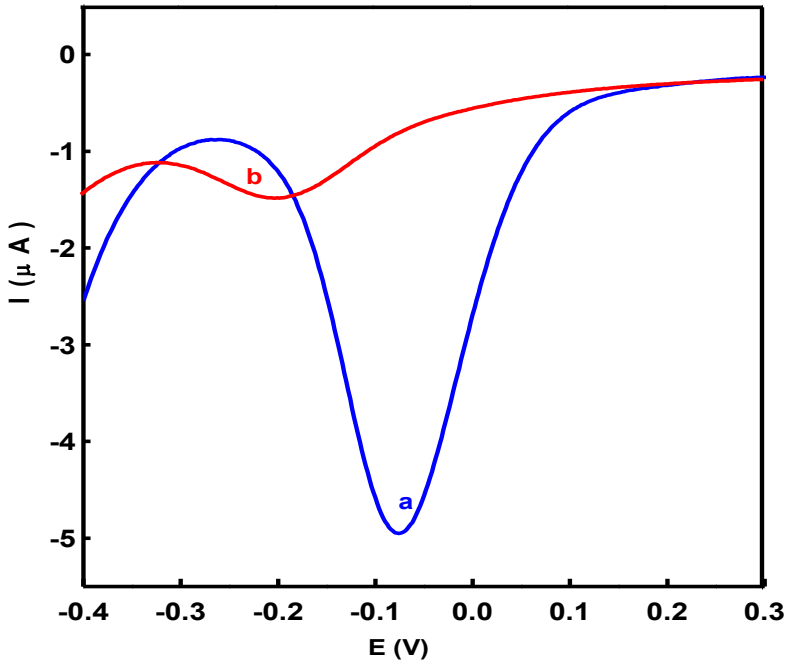

Fig. S17. Differential pulse voltammograms of **3** (0.5 mM) in the absence (a) and presence (b) of CT DNA (R = 5) at 25.0 ± 0.2 °C at 2 mV s^{-1} scan rate in 2% DMF/5mM Tris-HCl/50 mM NaCl buffer at pH 7.1.

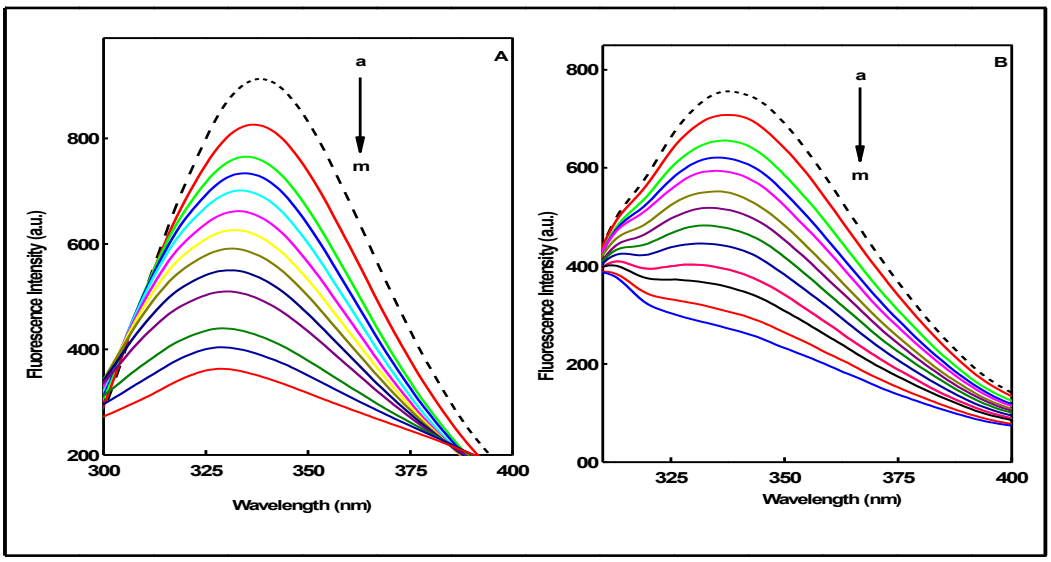

Fig. S18. Changes in the fluorescence spectra of BSA through the titration with complex **1** at 300 K (left, **A**) and 310 K (right, **B**). The concentration of BSA is 1×10^{-6} mol L^{-1}, and the concentration of **1** was varied from (a) 0.0 to (k) 3.5×10^{-6} mol L^{-1}; pH 7.4 and λ_{ex} 280 nm.

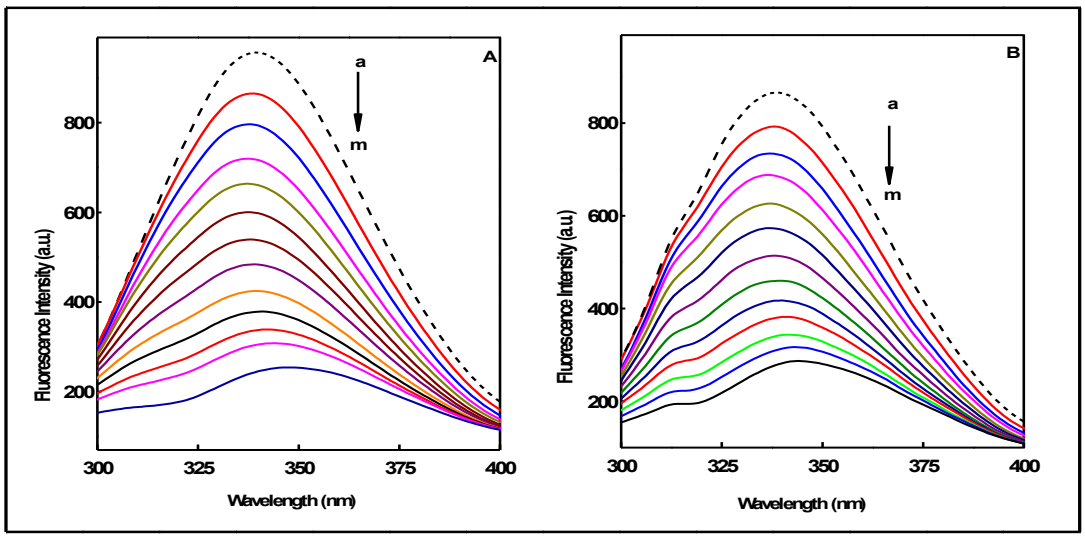

Fig. S19. Changes in the fluorescence spectra of BSA through the titration with complex **3** at 300 K (left, **A**) and 310 K (right, **B**). The concentration of BSA is 1×10^{-6} mol L^{-1}, and the concentration of **3** was varied from (a) 0.0 to (k) 3.5×10^{-6} mol L^{-1}; pH 7.4 and λ_{ex} 280 nm.

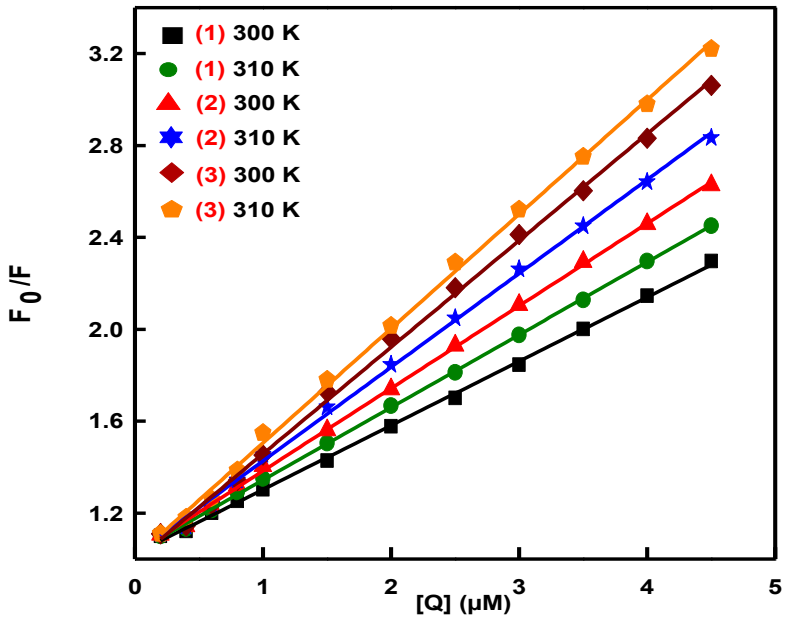

Fig. S20. The Stern-Volmer plots of BSA on different temperature for **1, 2** and **3**. λ_{ex} = 280 nm; pH = 7.4.

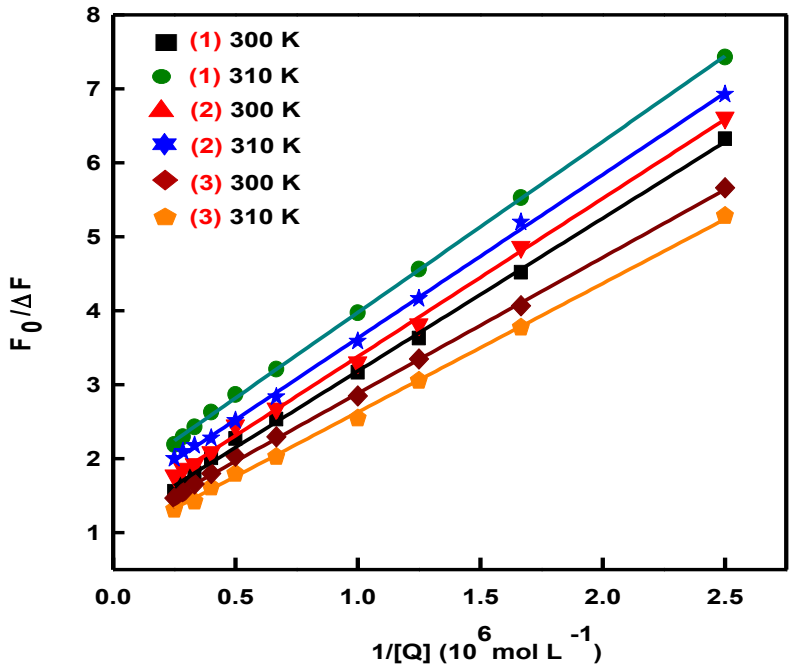

Fig. S21. The modified Stern-Volmer plots of BSA on different temperature for **1, 2** and **3**. λ_{ex} = 280 nm; pH = 7.4.

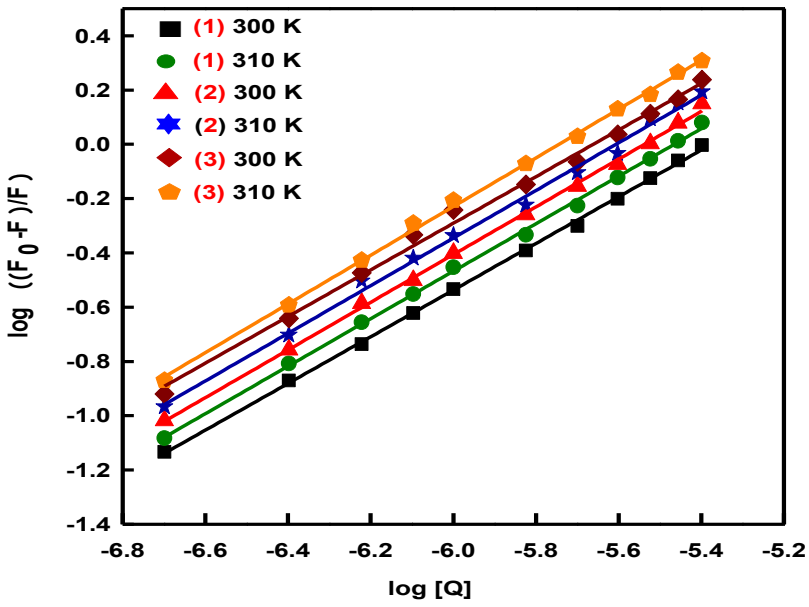

Fig. S22. Double-log plot of quenching effect of **1,2** and **3** on BSA fluorescence at pH = 7.4.

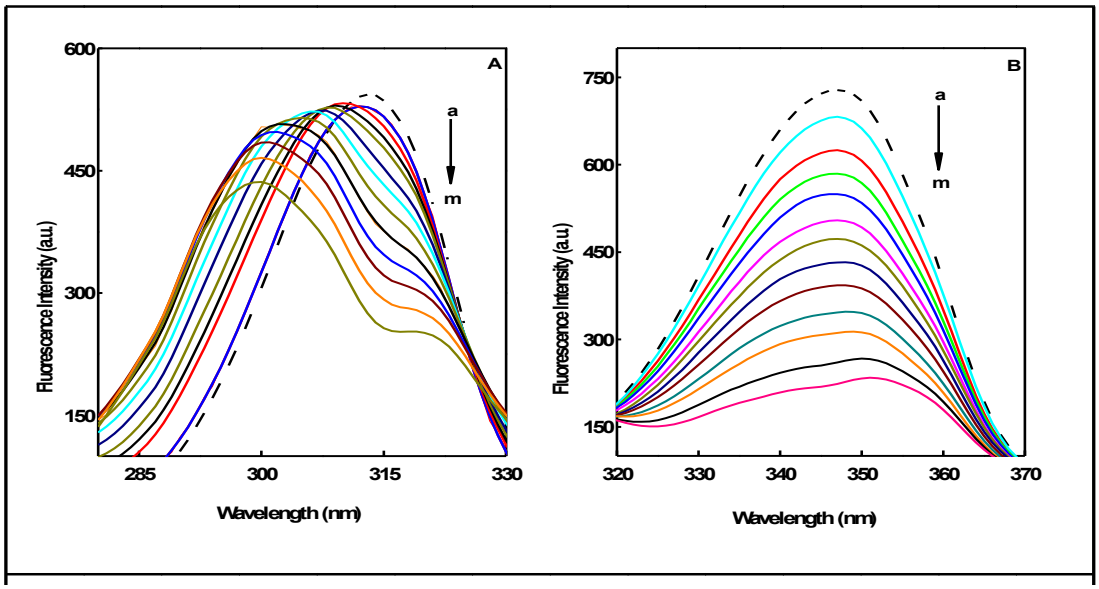

Fig. S23. Synchronous fluorescence spectra of BSA (1×10^{-6} mol L^{-1}) upon addition of **1**; $\Delta\lambda$ = 15 nm (**A**) and $\Delta\lambda$ = 60 nm (**B**). The concentration of **1** varied from (a) 0.0 to (j) 3.5×10^{-6} mol L^{-1}.

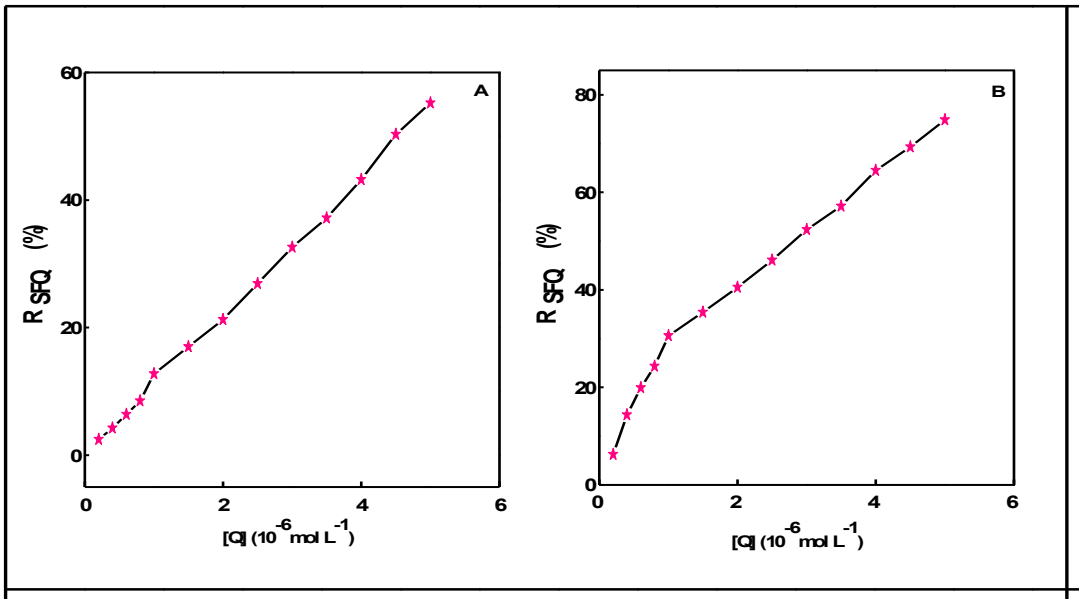

Fig. S24. Ratios of synchronous fluorescence quenching (R_{SFQ}) of BSA(1×10^{-6} mol L^{-1}) upon addition of **1**; $\Delta\lambda$ = 15 nm (**A**) and $\Delta\lambda$ = 60 nm (**B**). The concentration of **1** varied from (a) 0.0 to (j) 3.5×10^{-6} mol L^{-1}.

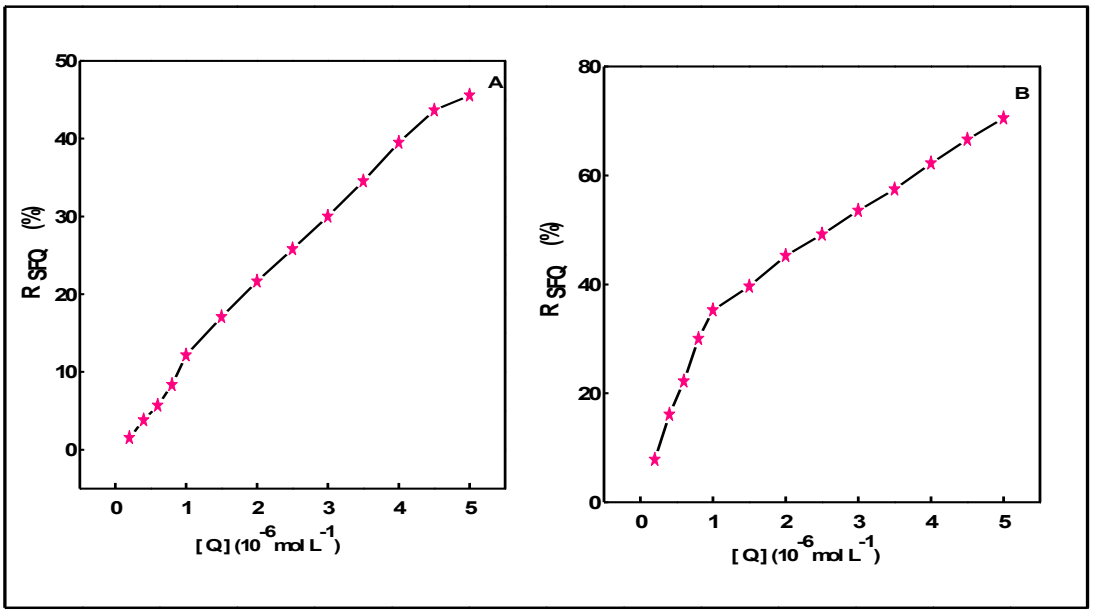

Fig. S25. Ratios of synchronous fluorescence quenching (R_{SFQ}) of BSA(1×10^{-6} mol L^{-1}) upon addition of **2**; $\Delta\lambda$ = 15 nm (**A**) and $\Delta\lambda$ = 60 nm (**B**). The concentration of **2** varied from (a) 0.0 to (j) 3.5×10^{-6} mol L^{-1}.

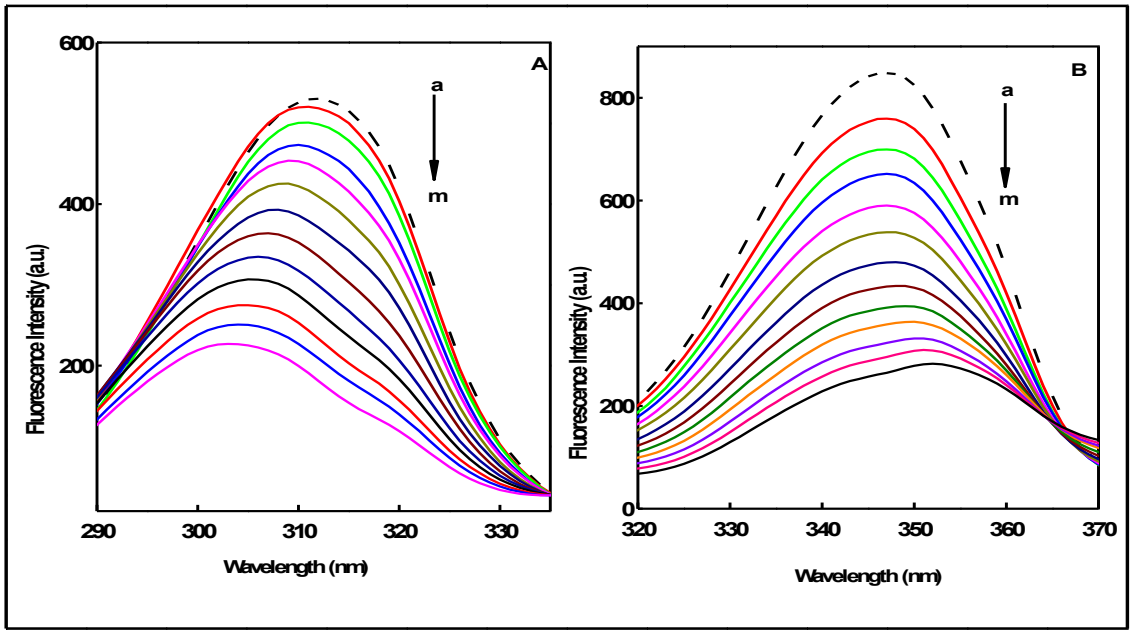

Fig. S26. Synchronous fluorescence spectra of BSA (1×10^{-6} mol L^{-1}) upon addition of **3**; $\Delta\lambda$ = 15 nm (**A**) and $\Delta\lambda$ = 60 nm (**B**). The concentration of **3** varied from (a) 0.0 to (j) 3.5×10^{-6} mol L^{-1}.

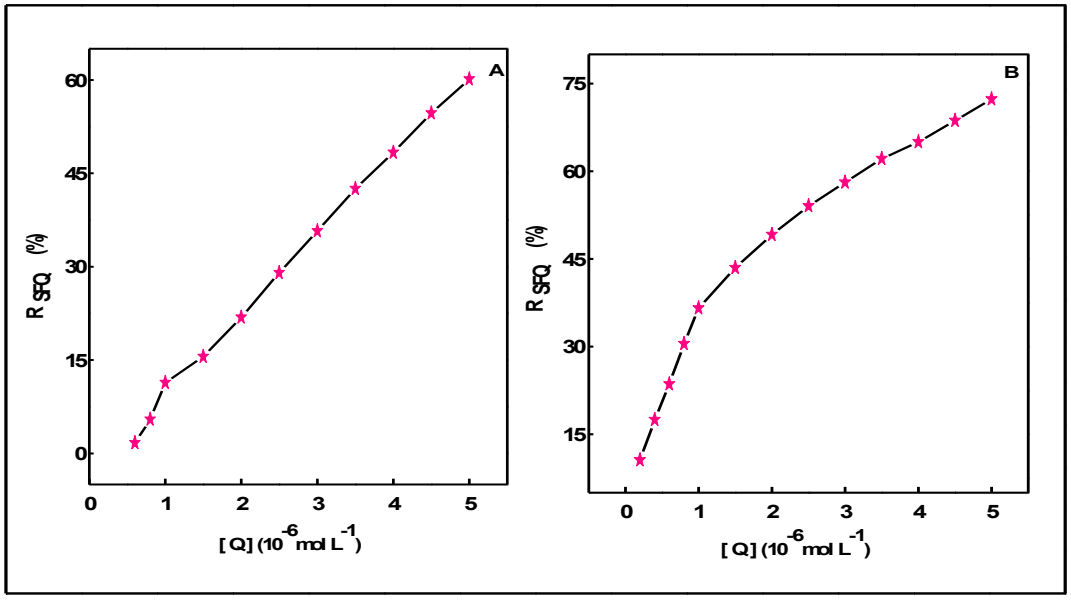

Fig. S27. Ratios of synchronous fluorescence quenching (R_{SFQ}) of BSA (1×10^{-6} mol L^{-1}) upon addition of **3**; $\Delta\lambda$ = 15 nm (**A**) and $\Delta\lambda$ = 60 nm (**B**). The concentration of **3** varied from (a) 0.0 to (j) 3.5×10^{-6} mol L^{-1}.

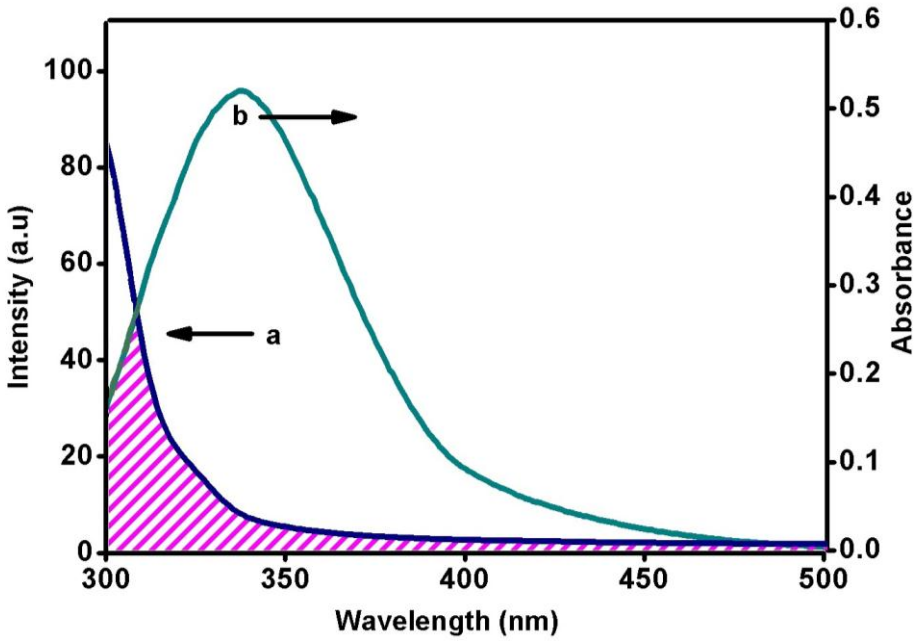

Fig. S28. Overlap of the fluorescence spectra (b) of BSA and the absorption spectra (a) of **1** , [BSA] = [Cu complex] = 1×10^{-6} mol L^{-1}.

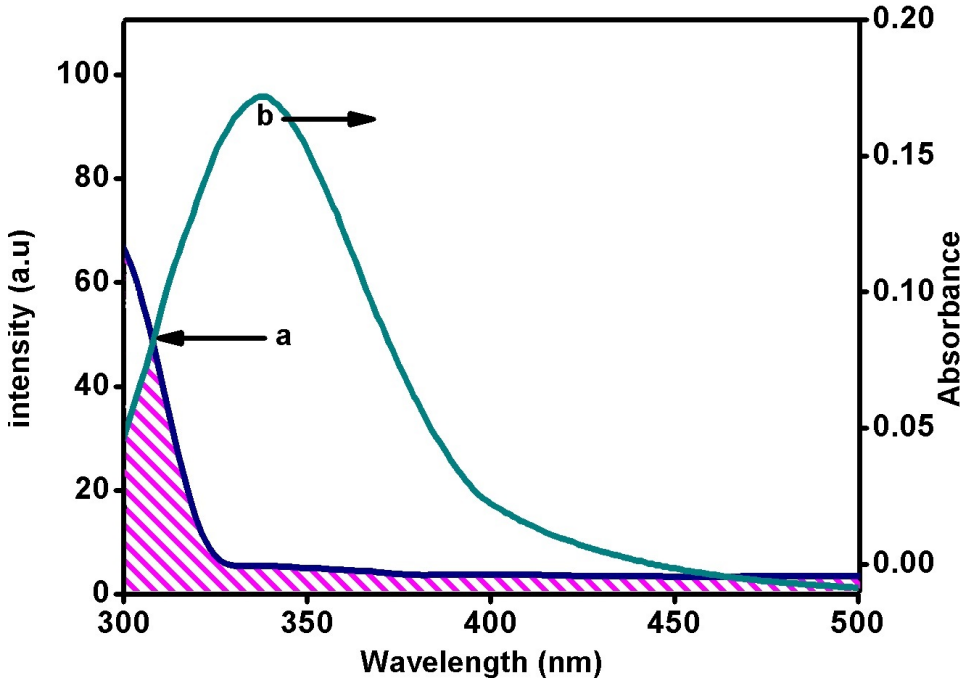

Fig. S29. Overlap of the fluorescence spectra (b) of BSA and the absorption spectra (a) of **2** , [BSA] = [Cu complex] = 1×10^{-6} mol L^{-1}.

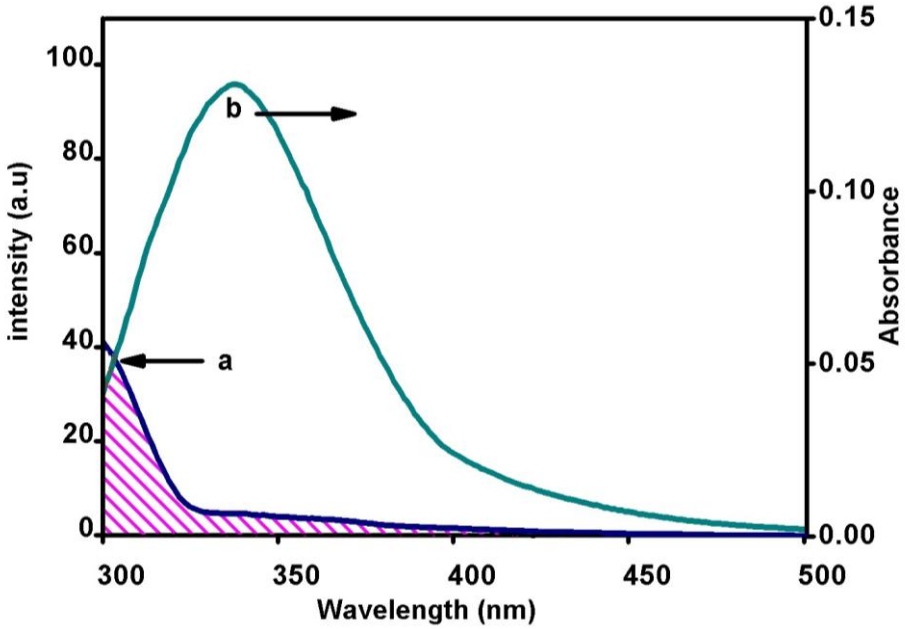

Fig. S30. Overlap of the fluorescence spectra (b) of BSA and the absorption spectra (a) of **3** , [BSA] = [Cu complex] = 1×10^{-6} mol L^{-1}.

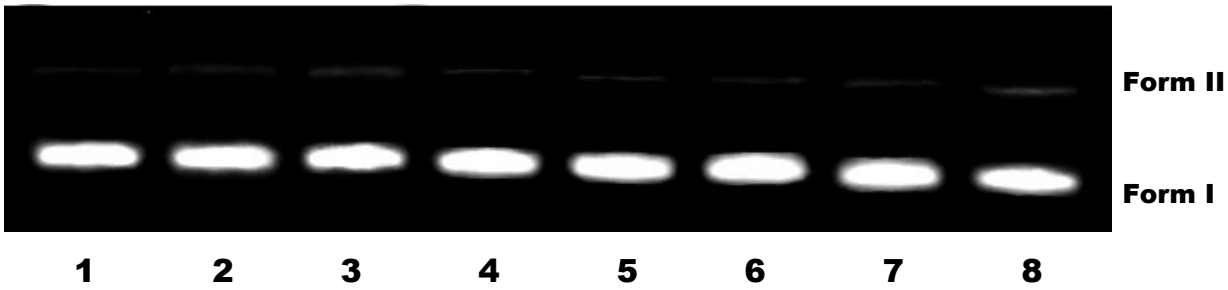

Fig. S31. Agarose gel showing cleavage of 20 μM SC pUC19 DNA incubated with **1** in 2% DMF/5 mM Tris-HCl/50 mM NaCl buffer at pH 7.1 and 37 °C for 1 h. Lane 1, DNA control; lanes 2-8, DNA+**1** (5, 10, 50, 100, 200, 300, 500 μM respectively). Forms I and II are supercoiled and nicked circular forms of DNA respectively.

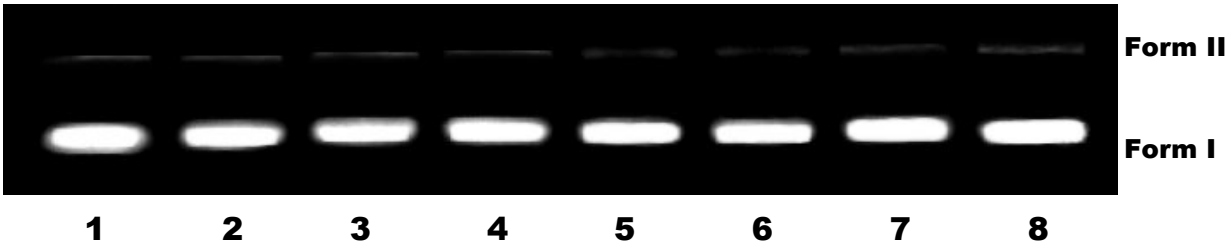

Fig. S32. Agarose gel showing cleavage of 20 μM SC pUC19 DNA incubated with **3** in 2% DMF/5 mM Tris-HCl/50 mM NaCl buffer at pH 7.1 and 37 °C for 1 h. Lane 1, DNA control; lanes 2-8, DNA+**3** (5, 10, 50, 100, 200, 300, 500 μM respectively). Forms I and II are supercoiled and nicked circular forms of DNA respectively.

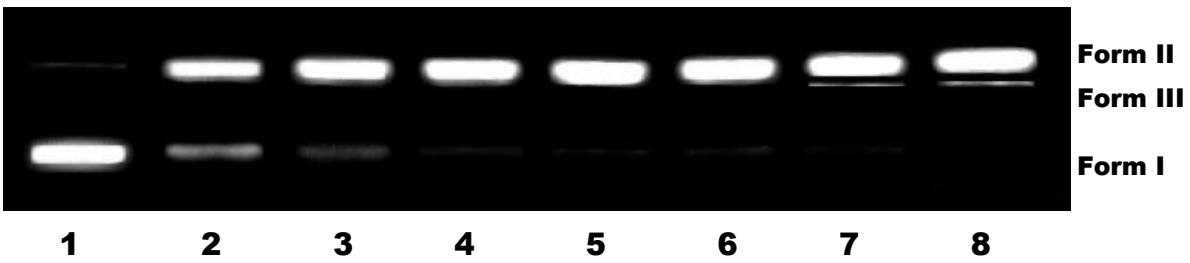

Fig. S33. Agarose gel showing cleavage of 20 μM SC pUC19 DNA incubated with **1** in 2% DMF/5 mM Tris-HCl/50 mM NaCl buffer at pH 7.1 and 37 °C in the presence of H_2O_2 (200 μM). Lane 1, DNA+H_2O_2; lanes 2-8, DNA+H_2O_2+**1** (1, 2, 3, 5, 10, 15, 20 μM respectively). Forms I, II and III are supercoiled, nicked circular and linear forms of DNA respectively.

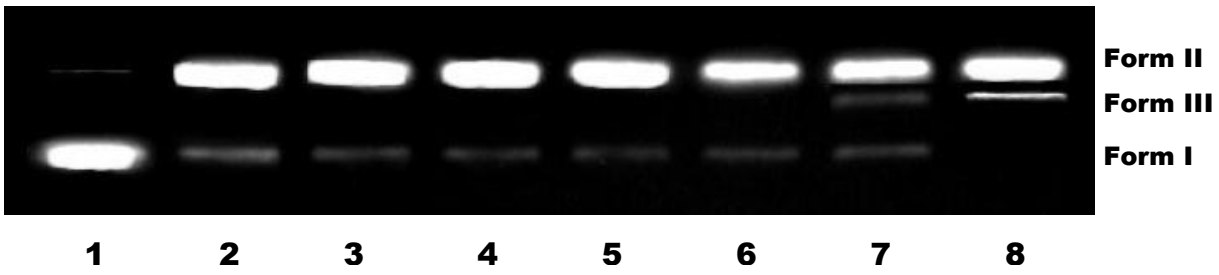

Fig. S34. Agarose gel showing cleavage of 20 μM SC pUC19 DNA incubated with **3** in 2% DMF/5 mM Tris-HCl/50 mM NaCl buffer at pH 7.1 and 37 °C in the presence of H_2O_2 (200 μM). Lane 1, DNA+H_2O_2; lanes 2-8, DNA+H_2O_2+**3** (1, 2, 3, 5, 10, 20, 30 μM respectively). Forms I, II and III are supercoiled, nicked circular and linear forms of DNA respectively.

Fig. S35. Gel electrophoresis diagram showing the cleavage of 20 μM SC pUC19 DNA by **1** (20 μM) in a 2% DMF/5 mM Tris-HCl/50 mM NaCl buffer at pH 7.1 and 37 °C in the presence of H_2O_2 (200 μM). with an incubation time of 2 h: lane 1, DNA control; lane 2, DNA+**1**; lane 3, DNA+**1**+H_2O_2; lane 4, DNA+**1**+H_2O_2+DMSO (20 μM); lane 5, DNA+**1**+ H_2O_2+SOD (0.5 units); lane 6, DNA+**1**+ H_2O_2+NaN_3 (100 μM); lane 7, DNA+**1**+ H_2O_2+Catalase (6 unit).

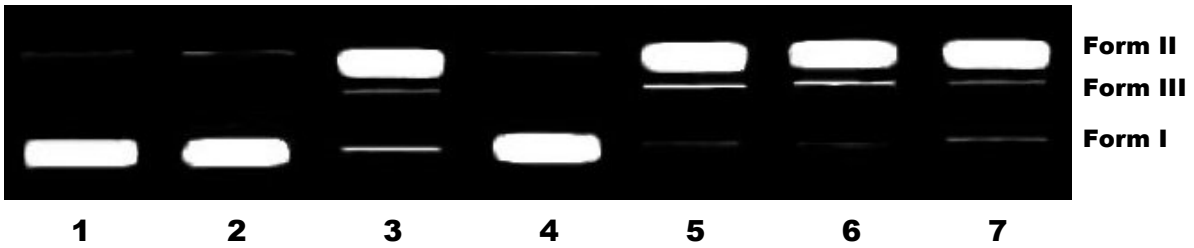

Fig. S36. Gel electrophoresis diagram showing the cleavage of 20 μM SC pUC19 DNA by **3** (30 μM) in a 2% DMF/5 mM Tris-HCl/50 mM NaCl buffer at pH 7.1 and 37 °C in the presence of H_2O_2 (200 μM). with an incubation time of 2 h: lane 1, DNA control; lane 2, DNA+**3**; lane 3, DNA+**3**+H_2O_2; lane 4, DNA+**3**+H_2O_2+DMSO (20 μM); lane 5, DNA+**3**+H_2O_2+SOD (0.5 units); lane 6, DNA+**3**+ H_2O_2+NaN_3 (100 μM); lane 7, DNA+**3**+ H_2O_2+Catalase (6 unit).

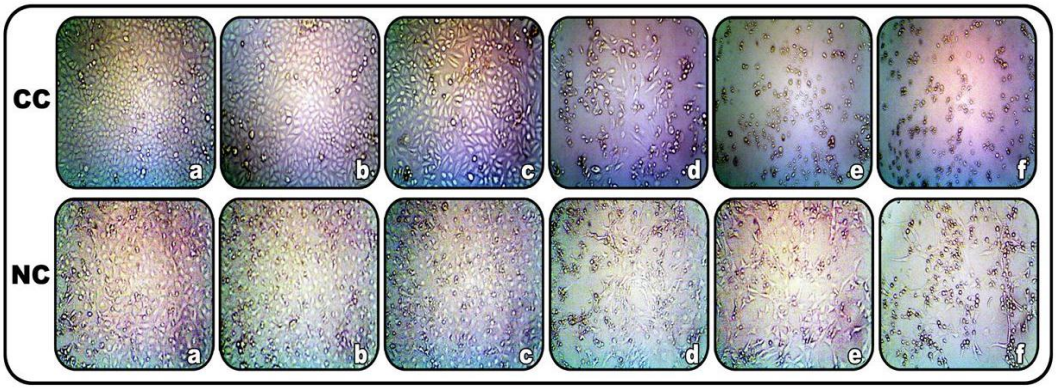

Fig. S37. Photomicrograph of human cervical carcinoma cell line (HeLa; **CC**) and normal mouse embryonic fibroblasts cell line (NIH 3T3; **NC**) after 48 h exposure with **1.**
CC (a, control; b, 0.25 μM; c, 2.5 μM; d, 25 μM; e, 50 μM; f, 100 μM).
NC (a, control; b, 0.1 μM; c, 1.0 μM; d, 10 μM; e, 50 μM; f, 100 μM).

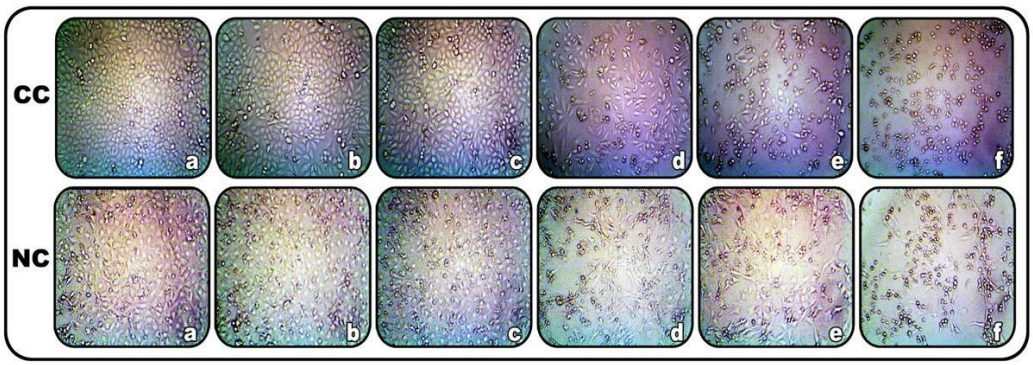

Fig. S38. Photomicrograph of human cervical carcinoma cell line (HeLa; **CC**) and normal mouse embryonic fibroblasts cell line (NIH 3T3; **NC**) after 48 h exposure with **3.**
CC (a, control; b, 0.25 μM; c, 2.5 μM; d, 25 μM; e, 50 μM; f, 100 μM).
NC (a, control; b, 0.1 μM; c, 1.0 μM; d, 10 μM; e, 50 μM; f, 100 μM).